https://doi.org/10.5194/amt-2021-80
Preprint. Discussion started: 24 March 2021

Atmospheric Measurement Techniques Discussions

Mie–Raman-Fluorescence lidar observations of aerosols during pollen season in the north of France

Igor Veselovskii[1], Qiaoyun Hu[2], Philippe Goloub[2], Thierry Podvin[2], Marie Choël[3], Nicolas Visez[4], Mikhail Korenskiy[1]

[1]*Prokhorov General Physics Institute of the Russian Academy of Sciences, Moscow, Russia.*

[2]*Univ. Lille, CNRS, UMR 8518 - LOA - Laboratoire d'Optique Atmosphérique, Lille, 59000, France*

[3]Univ. Lille, CNRS, UMR 8516 - LASIR - Laboratoire de Spectrochimie Infrarouge et Raman, 59000, Lille, France

[4]*Univ. Lille, CNRS, UMR 8522 - PC2A - Physicochimie des Processus de Combustion et de l'Atmosphère, 59000, Lille, France*

Correspondence: Igor Veselovskii (iveselov@hotmail.com)

Abstract

Multiwavelength Mie–Raman–fluorescence lidar of Lille University with the capability to measure three aerosol backscattering, two extinction coefficients and three linear depolarization ratios together with the fluorescence backscattering at 466 nm was used to characterize aerosols during the pollen season in the north of France for the period March – June 2020. The results of observations demonstrate that the presence of pollen grains in aerosol mixture leads to an increase of the depolarization ratio. Moreover, the depolarization ratio exhibits a strong spectral dependence increasing with wavelength, which is expected for the mixture containing fine background aerosols with low depolarization and strongly depolarizing pollen grains. High depolarization ratio correlates with the enhancement of the fluorescence backscattering, corroborating the presence of pollen grains. Obtained results demonstrate that simultaneous measurements of particle depolarization and fluorescence allows to separate dust, smoke particles and aerosol mixtures containing the pollen grains.

1. Introduction

Pollen grains represent a significant fraction of primary biological particles emitted from the biosphere into the atmosphere in certain seasons and locations (Fröhlich-Nowoisky et al., 2016). There has been a growing interest in pollen study in recent years, because they can affect human

Atmospheric Measurement Techniques
Discussions

health by causing allergy-related diseases and contribute to the cloud formation by acting as giant cloud condensation nuclei (CCN) (Diehl et al., 2001; Pope, 2010; D'Amato et al., 2014; Steiner et al., 2015; Lake et al., 2017; Mack et al., 2020). To investigate the processes of pollen transport and dispersion, the information about vertical distribution of pollen grains is needed, and this information can be obtained from lidar measurements. Pollen grains are large irregularly shaped particles of complicated morphology (Frenguelli, 2003), causing strong depolarization of the backscattered laser radiation, which provides a basis for their identification. The first profiling of pollen with depolarization lidar was reported by Sassen (2008, 2011). His measurements over Alaska revealed that linear depolarization ratio of birch pollen plumes at 0.694 nm can exceed 30%. Further studies of pollen with elastic backscatter lidar at 532 nm were reported by Noh et al. (2013 a,b) and by Sicard et al. (2016). Their measurements confirmed high depolarization ratio of pollen grains (particle depolarization ratios as high as 43% were observed for aerosol mixture containing *Platanus* and *Pinus* pollen). Moreover, pollen grains backscattering demonstrated strong diurnal cycle, being highest near the noon. The use of multiwavelength observations increases capability of lidar technique for aerosol characterization. In recent studies of Bohlmann et al. (2019) and Shang et al., (2020) measurements performed with Polly^{XT} lidar allowed to estimate mean values of the lidar ratios (about 45 sr and 55 sr at 355 and 532 nm respectively for birch pollen grains). The decrease of extinction and backscattering Angstrom exponents (EAE and BAE) during pollen episodes was also reported.

Atmospheric biological particles efficiently produce wideband fluorescence emission, when being exposed to UV radiation (Pohlker et al., 2012; Pan, 2015; Miyakawa et al., 2015), which offers an opportunity for monitoring them with fluorescence lidars. Nowadays, lidar spectrometers based on multianode photomultipliers allow a simultaneous detection of fluorescence backscattering in 32 spectral bins (Sugimoto et al., 2012; Reichardt et al., 2014, 2017; Saito et al., 2018). In particular, such lidar spectrometer was used in recent work of Saito et al. (2018) for remote measurement of the fluorescence spectrum of atmospheric pollen grains. The results demonstrate that, for 355 nm stimulating wavelength, the fluorescence spectra of different pollen grains have maxima in the 400–600 nm range and the intensity peak at around 460 nm.

To achieve the highest sensitivity of fluorescence detection, in many tasks it is preferable to use a single channel monitoring, where a part of the fluorescence spectrum is selected with a wideband interference filter (Immler et al, 2005; Rao et al., 2018; Li et al., 2019). In our recent

https://doi.org/10.5194/amt-2021-80
Preprint. Discussion started: 24 March 2021

publication (Veselovskii et al., 2020) we reported the results obtained from a modified Mie-Raman lidar (LILAS lidar system in Laboratoire d'optique Atmosphérique) with one additional fluorescence channel at 466 nm. Such an approach has proved high sensitivity, allowing to detect fluorescence signals from weak aerosol layers and to calculate the fluorescence backscattering coefficient from the ratio of fluorescence and nitrogen Raman backscatters, thus making it potentially attractive for pollen monitoring.

In the present research we combine capability of multiwavelength Mie–Raman lidar for providing three backscattering, two aerosol extinction coefficients and linear depolarization ratio at three wavelengths with single channel fluorescence measurements for characterization of aerosol mixtures containing pollen grains. The measurements reported were performed during March–June 2020 period at the Lille Atmospheric Observation Platform (https://www-loa.univ-lille1.fr/observations/plateformes.html?p=apropos) hosted by Laboratoire d'Optique Atmospherique, University of Lille, Hauts-de-France region.

2. Instrumentation

2.1 Mie-Raman-Fluorescence lidar

The measurements were performed using LILAS lidar system – a multiwavelength Mie-Raman lidar, based on a tripled Nd:YAG laser with a 20 Hz repetition rate and pulse energy of 70 mJ at 355 nm. The backscattered light is collected by a 40 cm aperture Newtonian telescope. The full geometrical overlap of the laser beam and the telescope FOV is achieved at approximately 1000 m and to obtain the information about particles at lower altitudes, part of the measurements were performed at an angle of 30 degrees to the horizon. The system is designed for a simultaneous detection of elastic and Raman backscattering, allowing the so called $3\beta+2\alpha+3\delta$ data configuration, including three particle backscattering (β_{355}, β_{532}, β_{1064}), two extinction (α_{355}, α_{532}) coefficients along with three particle depolarization ratios (δ_{355}, δ_{532}, δ_{1064}). The particle depolarization ratio δ, determined as a ratio of cross- and co-polarized components of the particle backscattering coefficient, was calculated and calibrated the same way as described in Freudenthaler et al. (2009). The description of the system can be found in the recent publication of Hu et al., (2019).

To perform fluorescence lidar measurements, the water vapor Raman channel at 408 nm was replaced by a fluorescence channel, whose spectrum is captured by a wideband filter centered at 466 nm and of 44 nm width (Veselovskii et al., 2020). The fluorescence measurements were performed during night time only. The aerosol extinction and backscattering coefficients at 355 and 532 nm were calculated from Mie-Raman observations (Ansmann et al., 1992), while β_{1064} was derived by the Klett method (Klett, 1985). The fluorescence backscattering coefficient β_F is calculated from the ratio of fluorescence and nitrogen Raman backscattering, as described in Veselovskii et al. (2020). This approach allows to evaluate the absolute values of β_F, if the relative sensitivity of the channels is calibrated and the nitrogen Raman scattering cross section is known. Corresponding uncertainty we estimate to be below 50%. Parameters of detectors were not changed during the campaign, so uncertainty of relative variations of β_F was significantly lower and was determined by the statistical errors of fluorescence measurements.

To characterize the efficiency of the fluorescence in respect to elastic scattering, the fluorescence capacity

$$G_F = \frac{\beta_F}{\beta_{532}} \tag{1}$$

is also used. This parameter depends on the relative humidity (RH), so information about RH is important for data analysis. Radiosonde measurements are used to monitor water vapor, as the water vapor channel is replaced by the fluorescence channel in current lidar configuration. The closest available radiosonde data are from Herstmonceux (UK) and Beauvecchain (Belgium) stations, located 160 km and 80 km away from the observation site respectively. These radiosonde data are not collocated with the lidar measurements, so only qualitative analysis of humidification effects was possible.

2.2 Pollen in situ sampling

Airborne pollen grains and spores were collected by a Hirst-type volumetric sampler (VPPS 2000, Lanzoni s.r.l). The pollen sampler was located on the campus of the University of Lille (France) on the rooftop of a 20-m-high building where the lidar instrument was operated. Ambient air was sampled at 10 L.min^{-1} flow rate, allowing the impaction of pollen and spores on an adhesive strip mounted on a rotating clockwork-driven drum. The impaction surface moves at 2 mm.h^{-1} behind the entrance slit, allowing a temporal resolution of 2 hours. The adhesive strip was substituted every 7 days after a full rotation of the drum, which is splitted into 7 parts, each corresponding to a day of monitoring. And then they are fixed on a microscope glass slide with gelatin and fuchsine dye. Pollen taxa were identified by light microscopy on the basis of their characteristic shape and size. Airborne pollen concentrations were expressed as a daily and dual hourly number of pollen grains per cubic meter of air.

Fig.1 shows the most abundant pollen taxa for the period from March to June 2020 in Lille. These include: *Betula* (54.8% of total pollen taxa over the period), *Fraxinus* (8.2%), *Quercus* (5.8%), *Urticaceae* (4.6%), *Salix* (4.5%) and *Cupressaceae* (4.1%). The same figure shows also the fluorescence backscattering β_F measured by lidar. The results presented are obtained by averaging all available data during the night and the maximal values in 500 – 1000 m range are shown. The highest fluorescence is observed in the end of March, when ash (*Fraxinus*) is the main pollinator. The period of intense birch (*Betula*) pollination (3-15 April 2020) correlates also with high β_F. Strong fluorescence observed for 5-10 May and 28 May–2 Jun periods, can be due to grass (*Poaceae*) pollen contribution. By the end of June, β_F decreases and becomes comparable with fluorescence backscattering of background aerosol. From Fig.1, we can conclude that there is no direct correlation between in situ and fluorescence lidar measurements, thus pollen observed in the boundary layer by the lidar are probably transported from other regions. However, comparing lidar and in situ observations, we should keep in mind, that maximum of pollen emission occurs near the noon, while lidar measurements were performed in the night.

3. Discrimination of pollen from other types of aerosol

3.1. Specific features of pollen containing aerosol mixture

In contrast to the observations performed over Alaska (Sassen, 2008, 2011) or Finland (Bohlmann et al., 2011), where pollen concentration was high due to boreal forests surrounding, the pollen loading in the north of France is significantly lower. Long-term lidar and sun photometer observations performed at Lille University demonstrate that local aerosol is mainly of continental type, with predominance of the fine mode particles and low depolarization ratio. The emission of large pollen grains, should lead to strong spectral dependence of the depolarization ratio, because the backscattering at 1064 is less sensitive to the fine background particles than at shorter wavelengths, thus particle depolarization ratio at 1064 nm (δ_{1064}) should be more sensitive to the presence of pollen grains, compared to δ_{355} and δ_{532}. The particle depolarization ratio δ of the mixture, containing background aerosol (*b*) and pollen (*p*), with corresponding depolarization ratios δ^b and δ^p, can be calculated as:

https://doi.org/10.5194/amt-2021-80
Preprint. Discussion started: 24 March 2021

$$\delta = \frac{\left(\frac{\delta^p}{1+\delta^p}\right)\beta^p + \left(\frac{\delta^b}{1+\delta^b}\right)\beta^b}{\frac{\beta^p}{1+\delta^p} + \frac{\beta^b}{1+\delta^b}} \qquad (2)$$

Here total backscattering $\beta = \beta^b + \beta^p$.

To estimate the dependence of depolarization of the aerosol mixture on the contribution of pollen to the backscattering coefficient $\frac{\beta_{532}^p}{\beta_{532}}$ at 532 nm, a simplified simulation was performed. Assuming that the depolarization ratios of pollen and background aerosol are spectrally independent and that δ^p=30% while δ^b=3%, the mixture depolarization ratios δ_{355}, δ_{532}, δ_{1064} were calculated as a function of $\frac{\beta_{532}^p}{\beta_{532}}$ using expression (2). The backscattering Angstrom exponents for background aerosol are assumed to be $A_{355/532}^{\beta} = A_{532/1064}^{\beta} = 1.5$, while for pollen $A_{355/532}^{\beta} = A_{532/1064}^{\beta} = 0$. Results of computation are shown in Fig.2. For low $\frac{\beta_{532}^p}{\beta_{532}}$ the depolarization ratio δ_{1064} significantly exceeds δ_{355} and δ_{532}. Spectral properties of the real mixture can be more complicated, due to possible spectral dependence of both δ^p and δ^b. Information on laboratory measured spectral dependence of depolarization ratios of pollen is rare. Cao et al. (2010) measured the linear depolarization ratio of several types of pollen in a chamber at 355, 532 and 1064 nm wavelengths. The results demonstrate a strong variation of spectral dependence for different taxa, and for most of the samples δ_{1064} exceeded δ_{355}. However, we should keep in mind that measurements in the chamber were performed at low RH, and depolarization ratios at higher RH may be different. Still, from Fig.2 we conclude that the increase of the particle depolarization ratio with wavelength can be an indication of the presence of large, irregularly-shaped pollen grains. We should recall that similar spectral dependence can be provided also by the dust particles in the aerosol mixture. However, as it will be shown later, pollen possesses significantly higher fluorescence capacity and this is how these particles can be discriminated from dust.

The presence of pollen should lead also to the decrease of the extinction and backscattering Angstrom exponents. EAE depends mainly on particle size, while BAE is sensitive also to the particle complex refractive index and shape, thus the measured profiles of EAE and BAE can present significant difference (Veselovskii et al., 2015). In our study we analyze the EAE and BAE for the wavelength pair 355/532 nm ($A^{\alpha}_{355/532}$ and $A^{\beta}_{355/532}$) only, because the extinction and backscattering coefficient involved are calculated from Mie–Raman observations.

When analyzing Mie-Raman-fluorescence lidar measurements of pollen containing aerosol mixtures, the numerous factors should be taken into account. These factors include the fluorescence of background aerosol and other non-pollen aerosols that have strong fluorescence capacity, for example, smoke particles. Dust particles can contribute to the increase of depolarization ratio and, finally, the hygroscopic growth can modify the particle parameters. All these factors will be considered in following sections.

3.2. Characteristics of background aerosol over observation site.

Long-term observations in Lille University demonstrate that aerosol over the observation site is mainly of continental type with predominance of the fine mode particles. Typical vertical profiles of the background aerosol parameters, observed on 3 June 2020, are given in Fig.3, showing aerosol elastic and fluorescence backscattering coefficients, lidar ratios, Angstrom exponents and depolarization ratios at three wavelengths. The RH from Beauvecchain (Belgium) radiosonde observations, was below 50% in the height range considered. Particle depolarization ratios at all three wavelengths are below 7%, indicating that contribution of pollen to the total backscattering is insignificant. This agrees with the low values of pollen concentration provided by in situ measurements (Fig.1a). The lidar ratios at both wavelengths (S_{355}, S_{532}) are close, varying in the 50-60 sr range, and the fluorescence capacity G_F is below 0.35×10^{-4}. The EAE and BAE ($A^{\alpha}_{355/532}$, $A^{\beta}_{355/532}$) are in the 1.5–2.0 range. The presence of pollen should lead to a deviation of the particle intensive parameters, such as the fluorescence capacity, depolarization ratio, EAE and BAE, from the typical values of background aerosol.

3.3 Identification of the smoke particles

During the observation period the smoke elevated layers transported over Atlantic were frequently detected. Smoke particles, are characterized by high fluorescence cross section (Reichardt et al., 2017; Veselovskii et al., 2020) and can interfere pollen fluorescence measurements. The temporal evolution of the range corrected lidar signal, volume depolarization ratio at 1064 nm and fluorescence backscattering for the smoke episode on the night 23 – 24 June 2020 are shown in Fig.4. During the night the smoke layer with low depolarization and high

https://doi.org/10.5194/amt-2021-80
Preprint. Discussion started: 24 March 2021

fluorescence is observed at approximately 5000 m height. Back trajectories (not shown) indicate that the layer is transported from Canada. Vertical profiles of the particle parameters for this episode are shown in Fig.5. The lidar ratio is about 50 sr at 355 nm, while the lidar ratio at 532 nm increases within the smoke layer from 60 sr to 80 sr. This increase of S_{532} occurs simultaneously with decrease of $A^{\alpha}_{355/532}$ from 1.5 to 0.75, indicating that the particle size inside the layer growths with height. Higher values of S_{532} in respect to S_{355} are typical characteristics for the aged smoke (e.g. Müller et al., 2005; Nicolae et al., 2013; Hu et al., 2019). The depolarization ratio decreases with wavelength from δ_{355}=10% to δ_{1064}=1.5%. Strong spectral dependence of depolarization ratio and, in particular, low values of δ_{1064}, are the features, allowing to identify the smoke layers. The extinction Angstrom exponent $A^{\alpha}_{355/532}$ in the center of layer is about 0.75, while $A^{\beta}_{355/532}$ is about 1.9 and shows no significant variation through the layer. High values of $A^{\beta}_{355/532}$ compared to $A^{\alpha}_{355/532}$ is another feature that will be used for aged smoke discrimination. Smoke fluorescence capacity is high, reaching up to $G_F=5*10^{-4}$ for the period of observations, and this is one more feature, allowing to separate smoke from other types of aerosol.

3.4 Identification of the dust particles

Presence of dust particles and pollen in the fine background aerosol leads to some common characteristics in the lidar data, such as the decrease Angstrom exponents and increase of depolarization ratios. However, pollen and dust can be separated by the fluorescence capacity. The vertical profiles of particle parameters during dust episode on 27 May are shown in Fig.6. The dust containing layer extends from 2000 m to 7000 m and the particle depolarization ratios δ_{1064} and δ_{532} in this layer are close to 20%. These values are lower than depolarization of pure dust. For example, Freudenthaler et al. (2009) for pure dust provide the values of 27% and 31% at 1064 nm and 532 nm wavelengths respectively, thus in our case transported dust particles may be mixed with local aerosols. The particle depolarization at 355 nm is not shown in the figure, because the scattering ratio in the dust layer was too low to compute δ_{355} reliably. The fluorescence capacity of particles in the dust layer is about 0.1×10^{-4} at 4000 m, which is factor 50 lower than G_F of the smoke in Fig.5. There is also a weak aerosol layer at 1600 m with β_{532} about 0.035 $Mm^{-1}sr^{-1}$. The fluorescence capacity in this layer is high ($G_F\approx2.0*10^{-4}$), suggesting that this layer may contain smoke or pollen particles.

https://doi.org/10.5194/amt-2021-80
Preprint. Discussion started: 24 March 2021

Atmospheric Measurement Techniques Discussions

3.5 Impact of particle hygroscopic growth

The vertical variation of observed aerosol properties may be a result of particle water uptake, which should be separated from the features related to pollen presence. Fig.7 shows the profiles of the particle parameters for the episode on 15 June 2020, when the aerosol hygroscopic growth could take place. In the height range 900–1500 m the fluorescence backscattering β_F is stable, while the elastic backscattering β_{532} increases by a factor 3. Radiosonde measurements in Herstmonceux (UK) in this height range demonstrate an increase of RH from about 75% to 85%, while lidar measured extinction and backscattering Angstrom exponents decrease from 1.5 to 1.3, corroborating the presence the particle hygroscopic growth. The depolarization ratio δ_{1064} at low altitudes exceeds δ_{355} and δ_{532}, which can be an indication of pollen presence. This is supported by significant fluorescence capacity (G_F=0.9×10^{-4} at 750 m).

The number of fluorescent particles in the 900–1500 m range, does not present significant changes (β_F is stable), so observed vertical variations, i.e. the decrease of depolarization ratios at all three wavelengths and the increase of lidar ratios S_{355} and S_{532} from 50 sr to 65 sr, are probably the result of water uptake by the particles. Water uptake does not change the number of fluorescent molecules, however the fluorescence capacity decreases in the process of the hygroscopic growth, so G_F can be a representative parameter of aerosol types only at the condition of low RH.

4. Results of lidar measurements in the presence of pollen

During March–June 2020, we had numerous measurement cases demonstrating the features in the profiles of the particle parameters, that can be attributed to pollen. For representative cases we have chosen observations with high depolarization ratio and high fluorescence backscattering. The same time, we omitted the days with high relative humidity, to minimize the impact of the hygroscopic growth effects. Below we consider several measurement cases representing different scenarios, in particular, the episodes when pollen concentration decreases with height (30-31 May, 1-2 June) and the episodes when pollen grains are well mixed inside the boundary layer (27-28 March and 21 April).

4.1. 30-31 May and 1-2 June 2020 observations

https://doi.org/10.5194/amt-2021-80
Preprint. Discussion started: 24 March 2021

Atmospheric Measurement Techniques
Discussions

The results of lidar measurements during the campaign in many episodes can be interpreted as decrease of pollen concentration with height. Vertical profiles of the main particle parameters for two representative cases in the nights of 30-31 May and 1-2 June 2020, are shown in Fig.8. The HYSPLIT back trajectory analysis (Stein et al., 2015) demonstrates that in 1000--2000 m height range the air masses were transported from the Northern Europe. At the ground level, the grass could be the main pollen contributor for this period, as shown in Fig 1. On 31 May (at 00:00 UTC) the RH measured by the radiosonde in Herstmonceux (UK) was about 40% at 500 m and it increased up to 70% at 2000 m. On 2 June the RH increased from approximately 40% to 60% in the same height range. For both nights the fluorescence backscattering decreases with height, indicating the decrease of the concentration of fluorescent particles (presumably pollen). This decrease of β_F correlates with decrement of the depolarization ratio at all three wavelengths. Particle depolarization δ_{1064} is the highest (about 15% at 750 m), while δ_{355} and δ_{532} are significantly lower. Such spectral dependence of depolarization ratio agrees with model calculation in Fig.2. The lidar ratios are available above 1250 m and for both cases, S_{355} and S_{532} increase with height. It indicates that the lidar ratios of pollen in the two considered cases can be quite low: below 40 sr at 355 nm and below 30 sr at 532 nm, considering that pollen concentration decreases with height, which is inferred from the features of depolarization ratio and fluorescence backscattering

The EAE for both nights is about 2.0 and does not show significant changes with height. The BAE is lower (about 1.5 at 1000 m) and for both nights it shows some increase in 1250–2250 m range. The BAE, in contrast to EAE, depends strongly on the particle refractive index and shape, thus it may demonstrate higher sensitivity to the changes in aerosol mixture composition. Recall that backscattering and extinction Angstrom exponents are related as:

$$A^{\beta}_{355/532} = A^{\alpha}_{355/532} + \frac{\ln(S_{532}/S_{355})}{\ln(355/532)} \quad (3)$$

Thus for $S_{355}>S_{532}$, which has been observed during pollen episodes, the $A^{\beta}_{355/532}$ is lower than $A^{\alpha}_{355/532}$. This is in contrast with smoke episodes, where $S_{355}>S_{532}$ and $A^{\beta}_{355/532} > A^{\alpha}_{355/532}$ (Fig.5).

If the depolarization ratios of pollen δ^p and background aerosol δ^b are known, the pollen backscattering coefficient β^p can be calculated. Such approach is widely used for the separation of contributions of dust and smoke particles (Sugimoto and Lee, 2006; Tesche et al., 2009) and

https://doi.org/10.5194/amt-2021-80
Preprint. Discussion started: 24 March 2021

the same technique was applied to separate pollen and background aerosol (Noh et al. 2013a; Sicard et al., 2016; Shang et al., 2020). For height independent depolarization ratios of pollen and background aerosol the pollen backscattering coefficient can be calculated as suggested by Tesche et al. (2009):

$$\beta^p = \beta \frac{(\delta - \delta^b)}{(\delta^p - \delta^b)} \frac{(1+\delta^p)}{(1+\delta)} \quad , \tag{4}$$

Here β and δ are backscattering coefficient and particle depolarization ratio of the mixture. The profiles of β^p_{532} and the relative contribution $\frac{\beta^p_{532}}{\beta_{532}}$ are shown in Fig.8(b,e). Computations were performed in assumption of height independent $\delta^p_{532} = 30\%$. For background aerosol, the values $\delta^b_{532} = 3\%$ for 30-31 May and $\delta^b_{532} = 5\%$ for 1-2 June were used. On 30 – 31 May contribution of pollen $\frac{\beta^p_{532}}{\beta_{532}}$ at 750 m is estimated as 30%. From Fig.2 the expected ratio $\delta_{1064}/\delta_{355}$ is about 2.3. It agrees with observed ratio, which is about 2.4.

The profiles of β_F and β^p_{532} in Fig.8(b, e) behave similarly, decreasing with height. Above 2000 m the decrease of β_F slows down due to the fluorescence of background aerosol. The profiles of the fluorescence capacity G_F and relative contribution $\frac{\beta^p_{532}}{\beta_{532}}$ also demonstrate a good correlation. Thus both depolarization and fluorescence techniques lead to the same conclusion: pollen concentration in the boundary layer for the considered episodes decreases with height.

4.2. 27 – 28 March and 21 April 2020 observations.

According to the in-situ pollen sampling at rooftop level, the maximal pollen content was detected during birch pollination period on 4–20 April. However, the maximal fluorescence backscattering of lidar data was observed in the end of March, when sampling shows an increase of ash (*fraxinus*) pollen emission. The temporal evolution of range corrected lidar signal, volume depolarization ratio at 1064 nm and fluorescence backscattering on 27-28 March night is shown in Fig.9. The main part of the aerosol is localized below 2000 m. The back trajectory analysis demonstrates the air masses in this episode were transported from the East Europe. In contrast with Fig.8, where fluorescence decreases with height, on 27 -28 March the fluorescent particles are

https://doi.org/10.5194/amt-2021-80
Preprint. Discussion started: 24 March 2021

Atmospheric Measurement Techniques Discussions

rather well mixed inside the PBL (planetary boundary layer). The fluorescence backscattering is high, exceeding 2.5×10^{-4} Mm^{-1}sr^{-1} and the volume depolarization at 1064 nm is above 15%. The vertical profiles of the particle parameters are shown in Fig.10. Radiosonde measurements (at both Beauvecchain and Herstmonceux sites) show that RH gradually increased with height from approximately 40% to 70% in 500–1750 m range.

Both the fluorescence backscattering and depolarization ratios do not demonstrate strong variations inside the 600–1500 m range. The maximum of fluorescence capacity exceeds 1.2×10^{-4}, which is significantly higher than G_F for background aerosol in Fig.3. The profiles of G_F and $\frac{\beta^p_{532}}{\beta_{532}}$ behave reasonably similar, the slight decrease of $\frac{\beta^p_{532}}{\beta_{532}}$ with height in respect to G_F can be due to dependence of depolarization ratio of pollen on RH.

Agreements between results obtained from depolarization and fluorescence techniques in Fig.8,10, corroborates the suggestion that the observed fluorescence is mainly due to the presence of pollen. However, in some episodes the particles with high fluorescence cross section, other than pollen, could interfere. In particular, such interference occurred in 20-23 April 2020 period. Fig.11 shows the vertical profiles of particle parameters measured on 21 April. The depolarization ratio δ_{1064}=22% at 750 m was one of the highest during campaign. The RH is low, increasing from 30% to 45% in 800–1500 m range, according to Herstmonceux radio sounding. The back trajectory analysis demonstrates, below 1500 m the air masses are transported from Spain, while at 2000 m the transportation is from the Northern Europe.

Fluorescence backscattering is stable in 500–1500 m range and the fluorescence capacity at 1000 m is about 1.5×10^{-4}, which is a typical value for the pollen. However, above 1250 m G_F starts to rise, reaching the value of 2.5×10^{-4} at 1750 m, meanwhile depolarization ratio decreases. Such high G_F is more typical for the smoke particles. The lidar ratios above 1250 m, as well as BAE, also increase. Such vertical variation of the intensive particle parameters was observed during 20-23 April period and it may indicate the presence of the biomass burning aerosol near the boundary layer top.

4.3. Separation of pollen and smoke layers

During the campaign we observed narrow layers with strong fluorescence. Two examples of such observations, in the nights 13-14 April and 16-27 May 2020, are shown in Fig.12. The

https://doi.org/10.5194/amt-2021-80
Preprint. Discussion started: 24 March 2021

white arrows on this figure point to the fluorescent layers. On 13 April, a weak aerosol layer (β_{532}≈0.6 Mm^{-1} for 23:00 – 00:00 UTC) is observed at the top of the PBL. This layer demonstrates volume depolarization ratios exceeding 10% and high fluorescence backscattering. On 26-27 May a weak layer with high fluorescence backscattering occurs between 3 km and 4 km. However, in contrast with the first case, it has low depolarization ratio, so the layers may have different nature. Fig.13 shows the vertical profiles of the particle parameters for these two cases. On 13-14 April the fluorescence backscattering below 1000 m is stable, while β_{532} rises, which can be the result of the particle water uptake. Above 1000 m, the depolarization ratio δ_{1064} increases up to 8%. Results in Fig.13a are averaged over 21:15–00:40 UTC temporal interval, but peak values of δ_{1064} between 23:00 and 00:00 exceeded 12%. Fluorescence backscattering increases simultaneously with the depolarization. The aerosol backscattering coefficient of fluorescent layer is too low for a reliable calculation of δ_{355} and δ_{532}, so only the profile of δ_{1064} is provided.

On 26-27 May the backscattering coefficient of the fluorescent layer at 3400 m is lower than in Fig.13a (β_{532}≈0.14 $Mm^{-1}sr^{-1}$), so the depolarization ratio δ_{1064} can be calculated only in the center of the layer and it is about 2%, which is significantly lower than that on 13-14 April. However, the fluorescence capacity on 26-27 May is up to 3.5×10^{-4}, which is typical for smoke. Thus, we can conclude that the fluorescent layer on 26-27 May contains the smoke particles, due to high G_F and low δ_{1064}. On 13-14 April, the fluorescence capacity is significantly lower (about 0.9×10^{-4}) and depolarization ratio δ_{1064} exceeds 10%, which is more typical for pollen. Due to low backscattering coefficients of the fluorescent layers in Fig.12, we are not able to provide a complete set of intensive parameters, such as Angstrom exponents and particle depolarization ratios at three wavelengths. However, based on the obtained fluorescence capacities and δ_{1064} values, we conclude that the fluorescent layers probably contain pollen grain in Fig.12a, and smoke particles in Fig.12b.

4.4 Aerosol classification based on polarization and fluorescence measurements.

Table 1 summarizes the results in the campaign, showing the aerosol parameters, such as particle depolarization and lidar ratios, extinction Angstrom exponent, fluorescence backscattering and capacity for several days in March–June 2020 observations period, when the contribution of pollen to the total particle backscattering was significant. All available night observations were averaged and results are given for heights with the highest particle depolarization. Lidar ratios varied approximately in 40--70 sr range, wherein normally S_{355} is greater than S_{532}. It must be emphasized that pollen lidar ratios may differ for different taxa and that the observed lidar ratios are not attributed to pure pollen, but to the aerosol–pollen mixture, so the values provided are influenced by the properties of background aerosol. Moreover, the shape of pollen grains depends on RH, (Heidemarie et al., 2018), which may also lead to the variation of pollen lidar ratios. In most of the cases, the depolarization ratio presents strong spectral dependence and increases with wavelength. This spectral dependence is probably the result of mixing of strongly depolarizing pollen grains with fine background aerosol. The maximal value of observed fluorescence capacity of pollen-aerosol mixture is 1.6×10^{-4}, which is significantly higher than that of background aerosol, but lower than fluorescence capacity of smoke.

The simultaneous observations of depolarization ratio and fluorescence capacity for different types of aerosol are summarized by Fig.14. On this plot, particle depolarization δ_{532} is plotted versus G_F. The diagram allows to separate four types of the particles: (i) dust particles – high δ_{532} and low G_F; (ii) pollen – high δ_{532} and high G_F; (iii) smoke – low δ_{532} and low G_F; (iiii) background aerosol (continental type) - low δ_{532} and low G_F. Points corresponding to the pollen mixture provide extended pattern, because parameters depend on the concentration of pollen in the aerosol mixture. The dust measurements are also scattered, because dust over the instrumentation site is long transported and mixed with local aerosol. Minimum G_F for dust is about 0.1×10^{-4} while for smoke maximal G_F is about factor 50 higher. The fluorescence capacity depends on the relative humidity, so strong scattering of measurement points can be partly also due to RH variations. Maximal values of G_F for pollen mixture were about 1.5×10^{-4}, and the corresponding depolarization ratios δ_{532} are about 18%. Thus, assuming that depolarization ratio of pure pollen is 30%, we can expect G_F for pure pollen to be about 2.5×10^{-4}, which is comparable with values for smoke.

Conclusion

We analyzed the measurements from a multiwavelength Mie-Raman-fluorescence lidar during March–June 2020 in the north of France, to reveal the features that can be attributed to pollen grains. Contrary to previous studies, where pollen was identified by the enhanced depolarization ratio at a single wavelength, our lidar system allowed to measure depolarization

https://doi.org/10.5194/amt-2021-80
Preprint. Discussion started: 24 March 2021

Atmospheric Measurement Techniques Discussions

ratios at three wavelengths, simultaneously with the fluorescence backscattering at 466 nm. In numerous episodes during the campaign, high values of the particle depolarization ratio at 1064 nm, exceeding 15%, were observed. Moreover, depolarization ratio had strong spectral dependence, being the highest at 1064 nm and lowest at 355 nm, which is expectable for big particles of irregular shape mixed with fine, low depolarizing background aerosol. The increase of particle depolarization correlated with enhancement of the fluorescence backscattering corroborating that in these episodes we observed aerosol mixtures containing pollen.

The lidar ratios of aerosol–pollen mixtures observed during campaign varied in a wide range. At low altitudes, where particle presented strong depolarization and fluorescence, in many cases we observed lidar ratios below 40 sr at both wavelengths. However, we had also cases when the lidar ratios at both wavelengths were in 50–60 sr range. Thus, at the moment we are not capable to specify lidar ratios for pure pollen and additional measurement campaigns in the locations with high pollen content are strongly desirable.

Obtained results demonstrate, that simultaneous measurements of particle depolarization and fluorescence allows to separate dust, smoke particles and pollen grains. Moreover, the fluorescence measurements provide additional information that can be used in aerosol classification schemes. However, further studies are needed to make this technique applicable for the quantitative pollen characterization. In the data analysis it is important to account for the process of water uptake by the particles, because hygroscopic growth increases backscattering of background aerosol and influences the pollen grain shape. In the presented lidar configuration, the water vapor channel was absent and radiosonde RH data were not collocated with lidar, which prevented us from performing a quantitative analysis of the hygroscopic effects. Since December 2020, we recovered the water vapor channel in upgraded configuration of the lidar. Moreover, we added one more fluorescence channel centered at 549 nm, which will be used in the next pollen campaign in 2021. This additional channel should improve discrimination of the pollen from other aerosols. In coming campaign we will try to correlate our results with pollen concentration at different location in Europe by using the transport model, e.g. SILAM (System for Integrated modeLling of Atmospheric coMposition) (Sofiev et al, 2013, 2015). The use of this model should help in identification of pollen type in our observations.

Acknowledgement

https://doi.org/10.5194/amt-2021-80
Preprint. Discussion started: 24 March 2021

We acknowledge funding from the CaPPA project funded by the ANR through the PIA under contract ANR-11-LABX-0005-01, the “Hauts de France” Regional Council and the European Regional Development Fund (ERDF). The “Réseau National de Surveillance Aérobiologique” (RNSA) and the “Association pour la Prévention de la Pollution Atmosphérique” (APPA) are gratefully acknowledged for providing Hirst-collected pollen grains identification and for assistance with the pollen data handling.

https://doi.org/10.5194/amt-2021-80
Preprint. Discussion started: 24 March 2021

Table 1. Lidar measured aerosol parameters, such as particle depolarization ratios (δ_{355}, δ_{532}, δ_{1064}), lidar ratios (S_{355}, S_{532}), extinction Angstrom exponent ($A^{\alpha}_{355/532}$), fluorescence backscattering coefficient (β_F) and fluorescence capacity (G_F) for several days during March – June 2020 period, when contribution of pollen to the total particle backscattering could be significant.

Day	Height, m	δ_{355}, %	δ_{532}, %	δ_{1064}, %	S_{355}, sr	S_{532}, sr	$A^{\alpha}_{355/532}$	β_F*10^{-4}, $Mm^{-1}sr^{-1}$	G_F*10^{-4}
27 Mar	1150	9	12	13	50	42	1.5	2.5	1.2
7 Apr	1150	13	13	13	60	60	1.25	1.0	1.3
8 Apr	1000	11	10	9	50	60	1.0	1.9	1.0
15 Apr	750	15	15	17	40	40	0.7	0.4	0.9
16 Apr	1250	15	15	15	-	-	-	0.6	1.6
19 Apr	650	8	10	14	58	48	1.35	1.2	0.9
20 Apr	1000	18	18	22	55	45	1.2	0.75	1.3
21 Apr	750	15	17	22	66	47	1.25	1.1	1.4
22 Apr	1000	18	18	22	70	55	1.2	0.9	1.5
23 Apr	1000	6	14	11	53	65	1.25	1.5	1.05
30 May	750	7	10	16	-	-	-	0.8	1.2
1 June	750	7	10	16	-	-	-	1.25	1.5

https://doi.org/10.5194/amt-2021-80
Preprint. Discussion started: 24 March 2021

References

Bohlmann, S., Shang, X., Giannakaki, E., Filioglou, M., Saarto, A., Romakkaniemi, S. and Komppula, M.: Detection and characterization of birch pollen in the atmosphere using multi-wavelength Raman lidar in Finland, Atmos. Chem. Phys. 19, 14559–14569, 2019. doi.org/10.5194/acp-19-14559-2019

Cao, X., Roy, G., and Bernier, R.: Lidar polarization discrimination of bioaerosols, Opt. Eng., 49, 116201, https://doi.org/10.1117/1.3505877, 2010.

D'Amato, P.G., Bergmann, K.C., Cecchi, L., Annesi-Maesano, I., Sanduzzi, A., Liccardi, G., Vitale, C., Stanziola, A., D'Amato, M.: Climate change and air pollution: Effects on pollen allergy and other allergic respiratory diseases. Allergo J 23, 32–38, 2014. https://doi.org/10.1007/s15007-014-0484-1

Diehl, K., Quick, C., Matthias-Maser, S., Mitra, S., Jaenicke, R.: The ice nucleating ability of pollen: Part I: Laboratory studies in deposition and condensation freezing modes. Atmospheric Research 58, 75–87, 2001. https://doi.org/10.1088/1748-9326/5/4/044015

Frenguelli, G.: Pollen structure and morphology, Advances in Dermatology and Allergology, 20, 200–204, 2003.

Freudenthaler,V., Esselborn, M.,Wiegner, M.,Heese, B., Tesche, M. and co-authors: Depolarization ratio profiling at severalwavelengths in pure Saharan dust during SAMUM 2006, *Tellus* 61B, 165–179, 2009.

Fröhlich-Nowoisky, J., Kampf, C. J., K., Weber, B., Huffman, J.A., Pöhlker, C., Andreae, M. O., Lang-Yona, N., et al.: Bioaerosols in the Earth system: Climate, health, and ecosystem interactions . Atmospheric Research, 182, 346-76, 2016. https://doi.org/10.1016/j.atmosres.2016.07.018.

Griffiths, P. T., Borlace, J.-S., Gallimore, P. J., Kalberer, M., Herzog, M., and Pope, F. D.: Hygroscopic growth and cloud activation of pollen: a laboratory and modelling study, Atmos. Sci. Lett., 13, 289–295, https://doi.org/10.1002/asl.397, 2012.

Heidemarie, S. U., Grímsson, F., Weber, M., Zetter, R., Hesse, M., Buchner, R., Svojtka, M., et Frosch-Radivo, A.:. *Illustrated Pollen Terminology*. 2^{e} éd. Springer International Publishing, 2018. http://www.springer.com/gp/book/9783319713649.

Hu, Q., Goloub, P., Veselovskii, I., Bravo-Aranda, J.-A., Popovici, I., Podvin, T., Haeffelin, M., Lopatin, A. , Dubovik, O., Pietras, C., Huang, X., Torres, B., and Chen, C.: Long-range-

https://doi.org/10.5194/amt-2021-80
Preprint. Discussion started: 24 March 2021

transported Canadian smoke plumes in the lower stratosphere over northern France, Atmos. Chem. Phys. 19, 1173 – 1193, 2019. doi.org/10.5194/acp-19-1173-2019.

Immler, F., Engelbart, D., Schrems, O.: Fluorescence from atmospheric aerosol detected by a lidar indicates biogenic particles in the lower stratosphere, Atmos. Chem. Phys. 5, 345–355, 2005.

Katifori, E., Alben, S., Cerda, E., Nelson, D. R., and Dumais, J.: Foldable structures and the natural design of pollen grains, P. Natl. Acad. Sci. USA, 107, 7635–7639, https://doi.org/10.1073/pnas.0911223107, 2010.

Klett J.D., "Lidar inversion with variable backscatter/extinction ratios", Appl.Opt. 24, 1638-1643, 1985.

Lake, I.R., Jones, N.R., Agnew, M., Goodess, C.M., Giorgi, F., Hamaoui-Laguel, L., Semenov, M.A., Solomon, F., Storkey, J., Vautard, R., Epstein, M.M.: Climate Change and Future Pollen Allergy in Europe. Environ Health Perspect 125, 385–391, 2017. https://doi.org/10.1289/EHP173

Li, B., Chen, S., Zhang, Y., Chen, H., Guo, P.: Fluorescent aerosol observation in the lower atmosphere with an integrated fluorescence-Mie lidar, J. Quant. Spectr. Rad. Transf., 227, 211–218, 2019.

Mack, S. M., Madl, A. K., Pinkerton, K. E.: Respiratory health effects of exposure to ambient particulate matter and bioaerosols, *Comprehensive Physiology*, 10, 1-20, 2020. https://onlinelibrary.wiley.com/doi/abs/10.1002/cphy.c180040

Miyakawa, T., Kanaya, Y., Taketani, F., Tabaru, M., Sugimoto, N., Ozawa, Y., and Takegawa, N.: Ground-based measurement of fluorescent aerosol particles in Tokyo in the spring of 2013: potential impacts of nonbiological materials on autofluorescence measurements of airborne particles, J. Geophys. Res. Atmos., 120, 1171–1185, 2015, doi:10.1002/2014JD022189.

Müller, D., Mattis, I., Wandinger, U., Ansmann, A., Althausen, D., Stohl, A.: Raman lidar observations of aged Siberian and Canadian forest fire smoke in the free troposphere over Germany in 2003: Microphysical particle characterization, J. Geophys. Res., 110, D17201, doi:10.1029/2004JD005756, 2005.

Nicolae D., A. Nemuc, D. Müller, C. Talianu, J. Vasilescu, L. Belegante, and A. Kolgotin: Characterization of fresh and aged biomass burning events using multi-wavelength Raman lidar and mass spectrometry, J. Geophys. Res. 118, 2956–2965, doi:10.1002/jgrd.50324, 2013.

Atmospheric Measurement Techniques Discussions
Open Access
EGU

Noh, M. Y., Müller, D., Lee, H., and Choi, T.: Influence of biogenic pollen on optical properties of atmospheric aerosols observed by lidar over Gwangju, South Korea, Atmos. Environ., 69, 139–147, https://doi.org/10.1016/j.atmosenv.2012.12.018, 2013a

Noh, Y. M., Lee, H., Mueller, D., Lee, K., Shin, D., Shin, S., Choi, T. J., Choi, Y. J., and Kim, K. R.: Investigation of the diurnal pattern of the vertical distribution of pollen in the lower troposphere using LIDAR, Atmos. Chem. Phys., 13, 7619–7629, https://doi.org/10.5194/acp-13-7619-2013, 2013b.

Pan, Y.-L.: Detection and characterization of biological and other organic-carbon aerosol particles in atmosphere using fluorescence, J. Quant. Spectr. Radiat. Trans. 150, 12–35, 2015.

Pohlker, C.; Huffman, J.A.; Poschl, U. Autofluorescence of atmospheric bioaerosols-fluorescent biomolecules and potential interferences. Atmos. Meas. Tech. **2012**, 5, 37–71.

Pope, F.D.: Pollen grains are efficient cloud condensation nuclei. Environ. Res. Lett. 5, 044015, 2010. https://doi.org/10.1088/1748-9326/5/4/044015

Rao, Z., He, T., Hua D, Wang, Y., Wang, X., Chen, Y., Le J.: Preliminary measurements of fluorescent aerosol number concentrations using a laser-induced fluorescence lidar, Appl. Opt. 57, 7211-7215, 2018.

Reichardt, J.: Cloud and aerosol spectroscopy with Raman lidar, J. Atm. Ocean. Tech., 31, 1946-1963, 2014.

Reichardt, J., Leinweber, R., Schwebe, A.: Fluorescing aerosols and clouds: investigations of co-existence, Proceedings of the 28th ILRC, Bucharest, Romania, 25-30 June, 2017.

Saito, Y., Ichihara, K., Morishita, K., Uchiyama, K., Kobayashi, F., Tomida, T.: Remote detection of the fluorescence spectrum of natural pollens floating in the atmosphere using a laser-induced-fluorescence spectrum (LIFS) lidar, Remote Sens., 10, 1533, 2018. doi:10.3390/rs10101533.

Sassen, K.: Boreal tree pollen sensed by polarization lidar: Depolarizing biogenic chaff, Geophys. Res. Lett., 35, L18810, https://doi.org/10.1029/2008GL035085, 2008.

Sassen, K.: Elliptical pollen corona from North American boreal paper birch trees (Betula papyrifera): strong fall orientations for near-spherical particles, Appl. Opt., 50, F1–F5, https://doi.org/10.1364/AO.50.0000F1, 2011.

Shang, X., Giannakaki, E., Bohlmann, S., Filioglou, M., Saarto, A., Ruuskanen, A., Leskinen, A., Romakkaniemi, S., Komppula, M.: Airborne pollen observations using a multi-wavelength

Raman polarization lidar in Finland: characterization of pure pollen types, Atm. Chem. Phys., 20, 15323–15339, 2020. doi.org/10.5194/acp-20-15323-2020.

Sofiev, M., Vira, J., Kouznetsov, R., Prank, M., Soares, J., Genikhovich, E.: Construction of the SILAM Eulerian atmospheric dispersion model based on the advection algorithm of Michael Galperin. Geoscientific Model Development 8, 3497–3522, 2015. https://doi.org/10.5194/gmd-8-3497-2015

Sicard, M., Izquierdo, R., Alarcón, M., Belmonte, J., Comerón, A., and Baldasano, J. M.: Near-surface and columnar measurements with a micro pulse lidar of atmospheric pollen in Barcelona, Spain, Atmos. Chem. Phys., 16, 6805–6821, https://doi.org/10.5194/acp-16-6805-2016, 2016.

Stein, A.F., Draxler, R.R, Rolph, G.D., Stunder, B.J.B., Cohen, M.D., and Ngan, F.: NOAA's HYSPLIT atmospheric transport and dispersion modeling system, Bull. Amer. Meteor. Soc., 96, 2059-2077, 2015. http://dx.doi.org/10.1175/BAMS-D-14-00110.1

Steiner, A. L., Brooks, S. D., Deng, C., Thornton, D. C.O., Pendleton, M. W., Bryant, V:. Pollen as atmospheric cloud condensation nuclei, *Geophysical Research Letters*, 2015GL064060, 2015. https://doi.org/10.1002/2015GL064060.

Sugimoto, N. and Lee, C. H.: Characteristics of dust aerosols inferred from lidar depolarization measurements at two wavelength, Appl. Opt., 45, 7468–7474, 2006.

Sugimoto, N., Huang, Z., Nishizawa, T., Matsui, I., Tatarov, B.: Fluorescence from atmospheric aerosols observed with a multichannel lidar spectrometer," Opt. Expr. 20, 20800-20807, 2012.

Tesche, M., Ansmann, A., Müller, D., Althausen, D., Engelmann, R., Freudenthaler, V., and Groß, S.: Vertically resolved separation of dust and smoke over Cape Verde using multiwavelength Raman and polarization lidars during Saharan Mineral Dust Experiment 2008, J. Geophys. Res., 114, D13202, doi:10.1029/2009JD011862, 2009.

Veselovskii, I., Whiteman, D. N., Korenskiy, M., Suvorina, A., Kolgotin, A., Lyapustin, A., Wang, Y., Chin, M., Bian, H. Kucsera, T. L., Perez-Ramirez, D., Holben, B.: Characterization of forest fire smoke event near Washington, D.C. in Summer 2013 with multi-wavelength lidar. Atmos. Chem. Phys. 15, 1647–1660, 2015.

Veselovskii, I., Hu, Q., Goloub, P., Podvin, T., Korenskiy, M., Pujol, O., Dubovik, O., Lopatin, A.: Combined use of Mie-Raman and fluorescence lidar observations for improving aerosol

https://doi.org/10.5194/amt-2021-80
Preprint. Discussion started: 24 March 2021

characterization: feasibility experiment, Atm. Meas. Tech., 13, 6691–6701, 2020. doi.org/10.5194/amt-13-6691-2020.

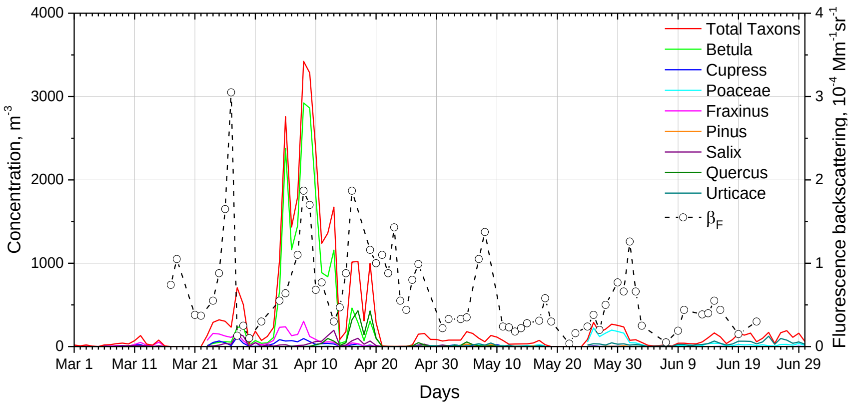

Fig.1. Daily concentration of most abundant pollen taxa, for the period March–June 2020 in Lille from in situ measurements on the rooftop. Open symbols show fluorescence backscattering β_F measured by lidar. Lidar measurements are averaged over night and maximal value in 500–1000 m range is shown.

https://doi.org/10.5194/amt-2021-80
Preprint. Discussion started: 24 March 2021

Atmospheric Measurement Techniques Discussions

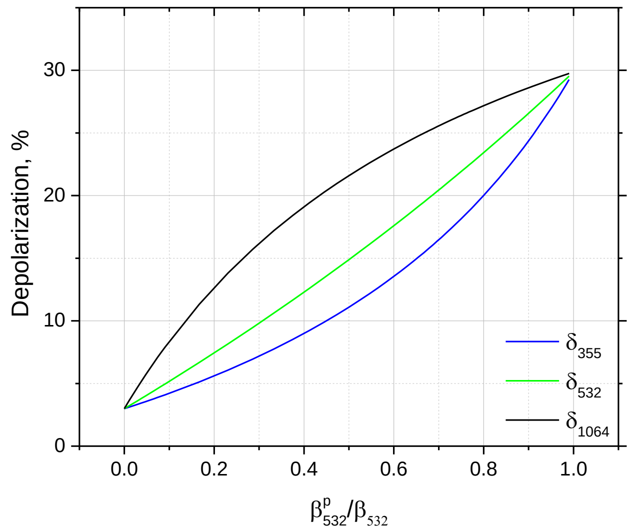

Fig.2. Depolarization ratios at 355, 532 and 1064 nm as a function of pollen contribution to the total backscattering coefficient $\frac{\beta^p_{532}}{\beta_{532}}$. Depolarization ratios of pollen (δ^p) and background aerosol (δ^b) are assumed to be spectrally independent, with values of δ^p=0.3 and δ^b=0.03. The backscattering coefficient of pollen is spectrally independent, while for background aerosol the backscattering Angstrom exponents $A^\beta_{355/532} = A^\beta_{532/1064} = 1.5$ were used.

https://doi.org/10.5194/amt-2021-80
Preprint. Discussion started: 24 March 2021

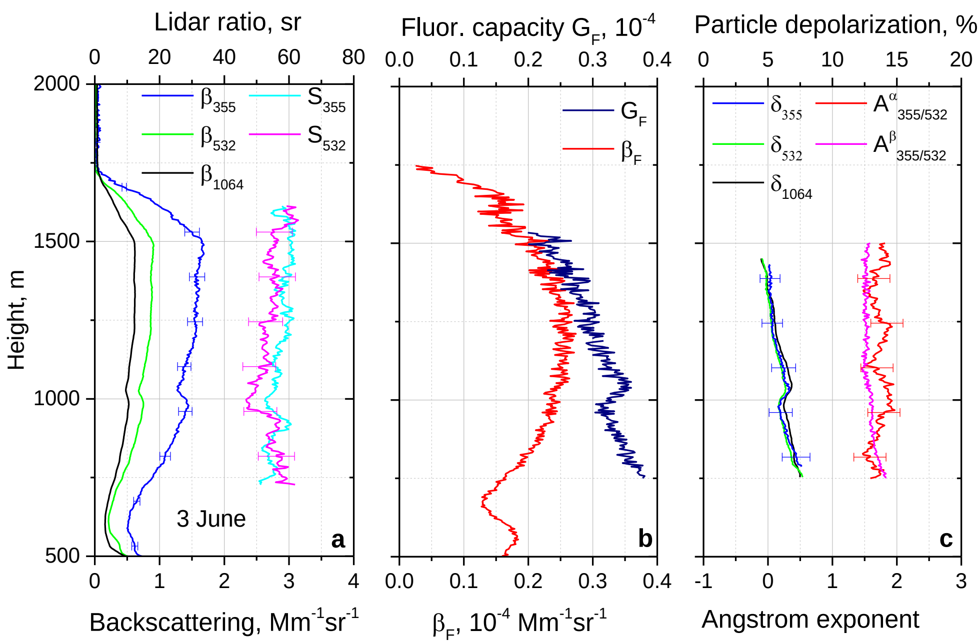

Fig.3. Measurements in the condition of background aerosol predominance. Vertical profiles of (a) backscattering coefficients β_{355}, β_{532}, β_{1064} and lidar ratios S_{355}, S_{532}; (b) fluorescence backscattering β_F and fluorescence capacity $G_F = \beta_F/\beta_{532}$; (c) particle linear depolarization ratios δ_{355}, δ_{532}, δ_{1064} together with extinction and backscattering Angstrom exponents $A^{\alpha}_{355/532}$, $A^{\beta}_{355/532}$ on 3 June 2020 for 20:30 – 23:00 UTC. Measurements were performed at 30 degree to the horizon.

https://doi.org/10.5194/amt-2021-80
Preprint. Discussion started: 24 March 2021

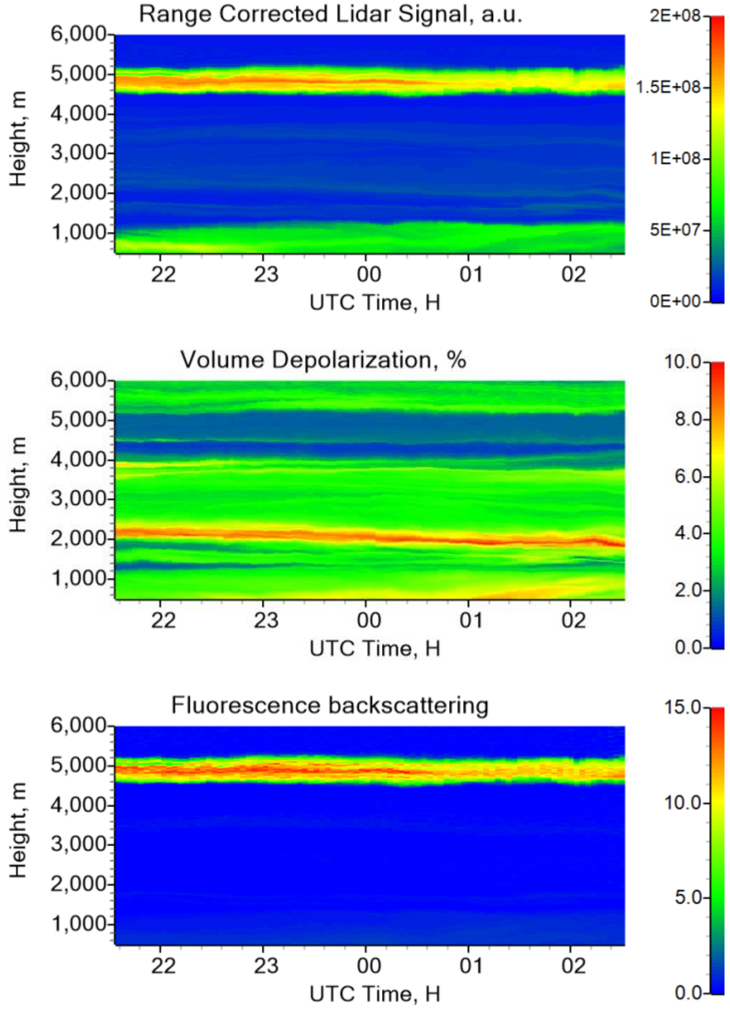

Fig.4. Range corrected lidar signal at 1064 nm, volume depolarization ratio at 1064 nm and fluorescence backscattering coefficient (in 10^{-4} $Mm^{-1}sr^{-1}$) on 23-24 June 2020.

https://doi.org/10.5194/amt-2021-80
Preprint. Discussion started: 24 March 2021

Atmospheric Measurement Techniques
Discussions

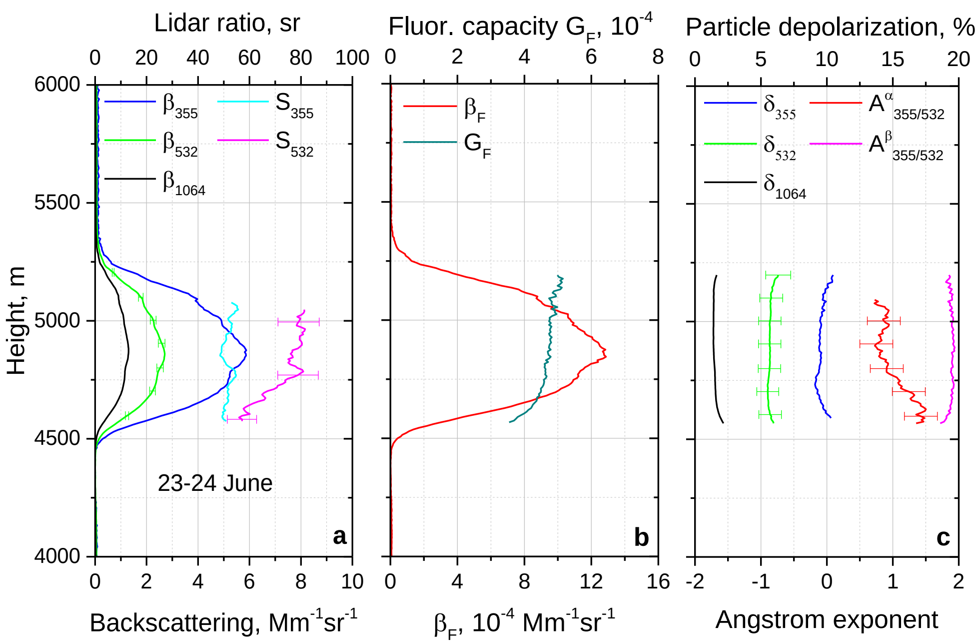

Fig.5. Vertical profiles of (a) backscattering coefficients β_{355}, β_{532}, β_{1064}, lidar ratios S_{355}, S_{532}; (b) fluorescence backscattering coefficient β_F, fluorescence capacity G_F; and (c) particle depolarization ratios δ_{355}, δ_{532}, δ_{1064} together with the extinction and backscattering Angstrom exponents $A^{\alpha}_{355/532}$, $A^{\beta}_{355/532}$ on the night 23-24 June 2020 for 21:30 – 02:30 UTC.

https://doi.org/10.5194/amt-2021-80
Preprint. Discussion started: 24 March 2021

Atmospheric Measurement Techniques
Discussions

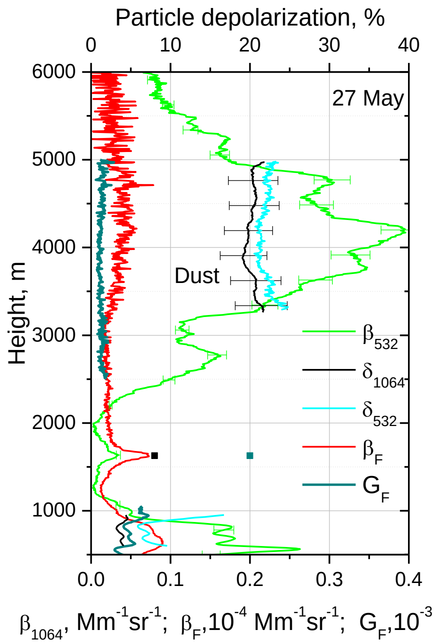

Fig.6. Lidar measurements during dust episode. Vertical profiles of particle β_{1064} and fluorescence β_F backscattering coefficients, fluorescence capacity G_F and particle depolarization ratios δ_{1064}, δ_{532} on 27 May 2020 for 21:00–23:00 UTC.

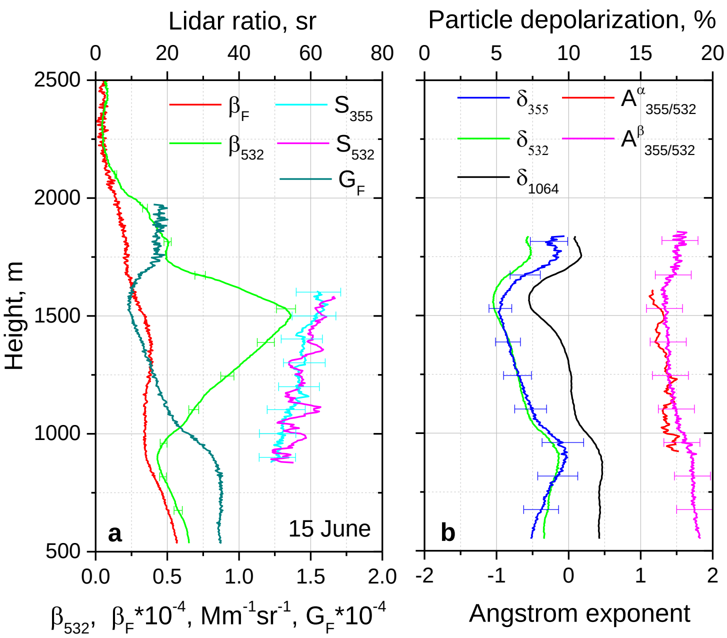

Fig.7. Lidar measurements in the condition of the aerosol hygroscopic growth in 900-1500 m height range. Vertical profiles of (a) particle β_{532} and fluorescence β_F backscattering coefficients, fluorescence capacity G_F, lidar ratios S_{355}, S_{532} and (b) particle depolarization ratios δ_{355}, δ_{532}, δ_{1064} together with extinction $A^{\alpha}_{355/532}$ and backscattering $A^{\beta}_{355/532}$ Angstrom exponents measured on 15 June 2020 for 22:00 – 24:00 UTC.

https://doi.org/10.5194/amt-2021-80
Preprint. Discussion started: 24 March 2021

Atmospheric Measurement Techniques
Discussions
Open Access
EGU

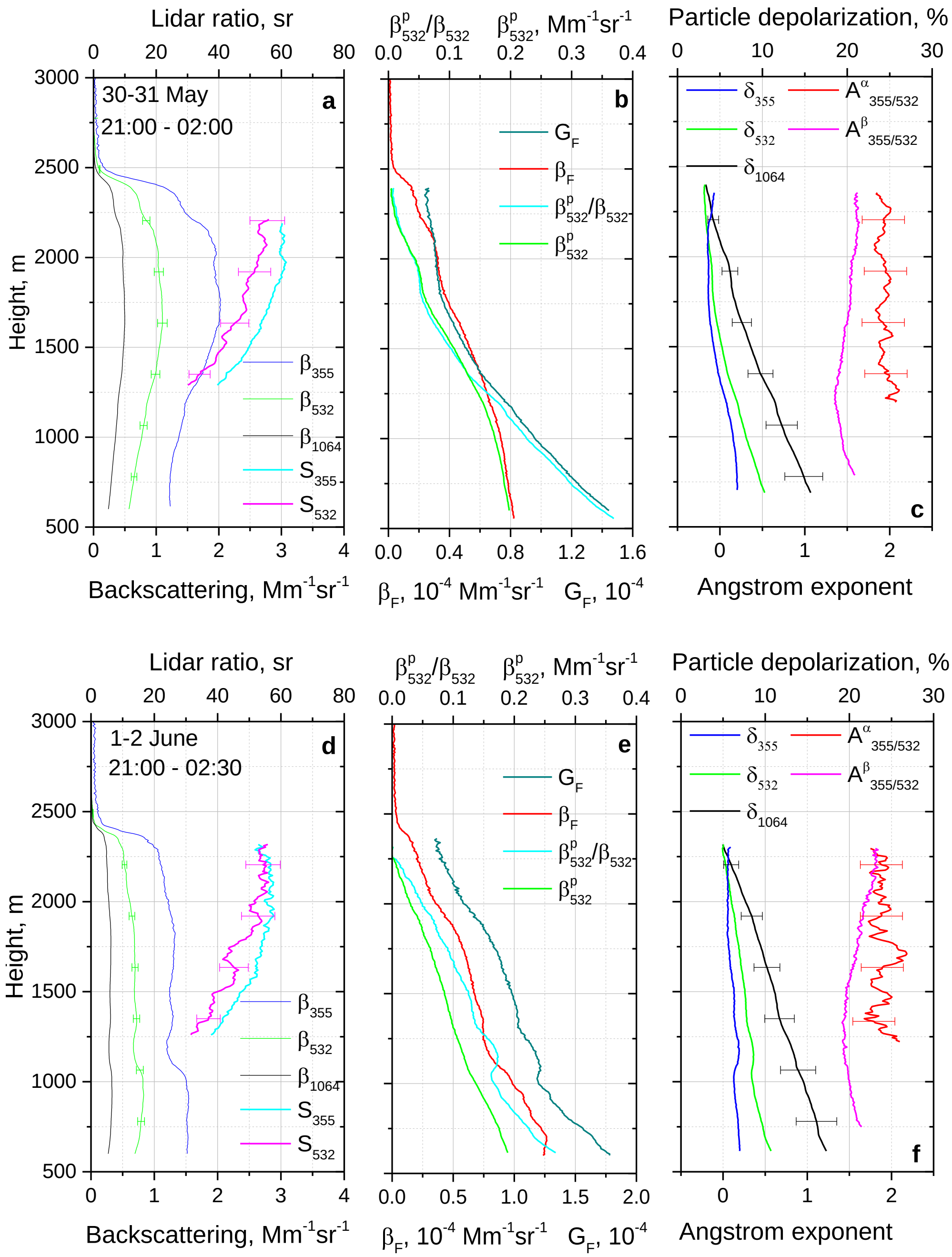

Fig.8. Vertical profiles of (a, d) particle backscattering coefficients β_{355}, β_{532}, β_{1064} and lidar ratios S_{355}, S_{532}, (b, e) fluorescence backscattering coefficient β_F, fluorescence capacity G_F, pollen

https://doi.org/10.5194/amt-2021-80
Preprint. Discussion started: 24 March 2021

Atmospheric Measurement Techniques Discussions

backscattering coefficient β_{532}^{p} and its contribution to the total backscattering $\frac{\beta_{532}^{p}}{\beta_{532}}$; (c, f) particle depolarization ratios δ_{355}, δ_{532}, δ_{1064} together with extinction $A_{355/532}^{\alpha}$ and backscattering $A_{355/532}^{\beta}$ Angstrom exponents on (a-c) 30 - 31 May 2020 for 21:00 – 02:00 UTC and on (d-f) 1-2 June 2020 for 21:00 – 02:30 UTC. Profiles of β_{532}^{p} and $\frac{\beta_{532}^{p}}{\beta_{532}}$ were computed in assumption of $\delta_{532}^{p} = 30\%$. The depolarization ratios of the background aerosol δ_{532}^{b} is measured/assumed to be 3% on 30 May and 5% on 1 May.

https://doi.org/10.5194/amt-2021-80
Preprint. Discussion started: 24 March 2021

Atmospheric Measurement Techniques
Discussions

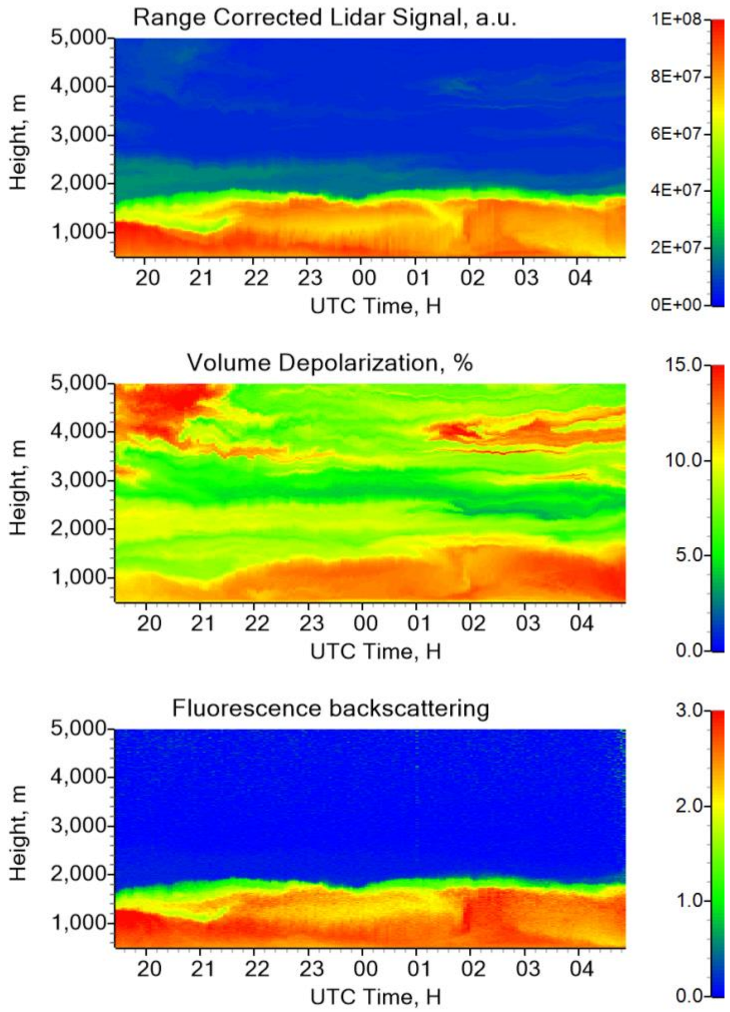

Fig.9. Range corrected lidar signal at 1064 nm (upper panel), volume depolarization ratio at 1064 nm (middle panel) and fluorescence backscattering coefficient (in 10^{-4} $Mm^{-1}sr^{-1}$, lower panel) measured on 27-28 March 2020.

https://doi.org/10.5194/amt-2021-80
Preprint. Discussion started: 24 March 2021

Atmospheric Measurement Techniques
Discussions

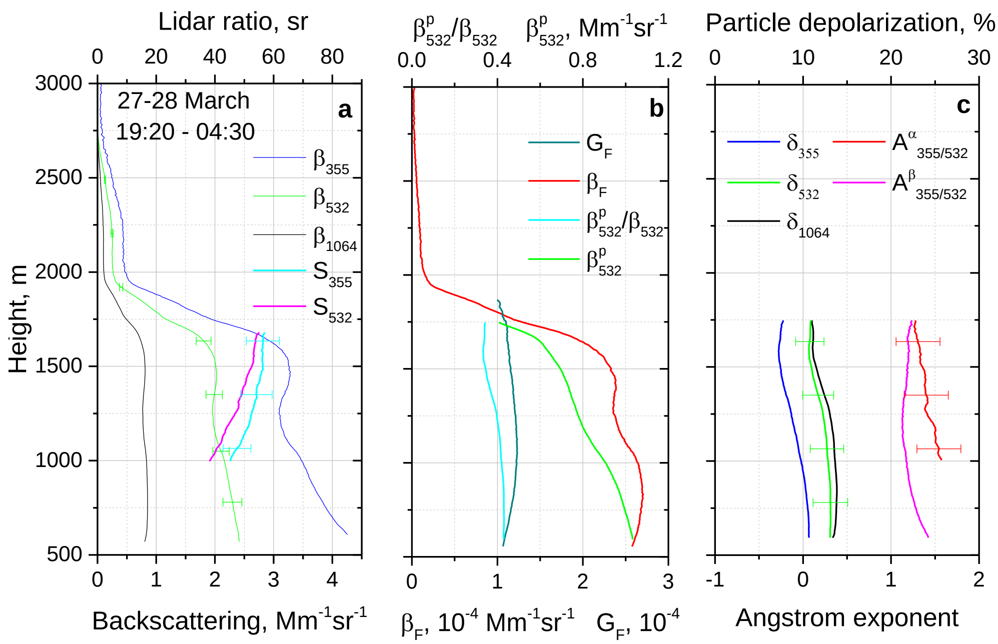

Fig.10. Vertical profiles of (a) particle backscattering coefficients β_{355}, β_{532}, β_{1064} and lidar ratios S_{355}, S_{532}; (b) fluorescence backscattering coefficient β_F, fluorescence capacity G_F, pollen backscattering coefficient β^p_{532} and its contribution to the total backscattering $\frac{\beta^p_{532}}{\beta_{532}}$; (c) particle depolarization ratios δ_{355}, δ_{532}, δ_{1064} together with extinction $A^{\alpha}_{355/532}$ and backscattering $A^{\beta}_{355/532}$ Angstrom exponents measured on 27 - 28 March 2020 for19:20 – 04:30 UTC.

https://doi.org/10.5194/amt-2021-80
Preprint. Discussion started: 24 March 2021

Atmospheric Measurement Techniques
Discussions

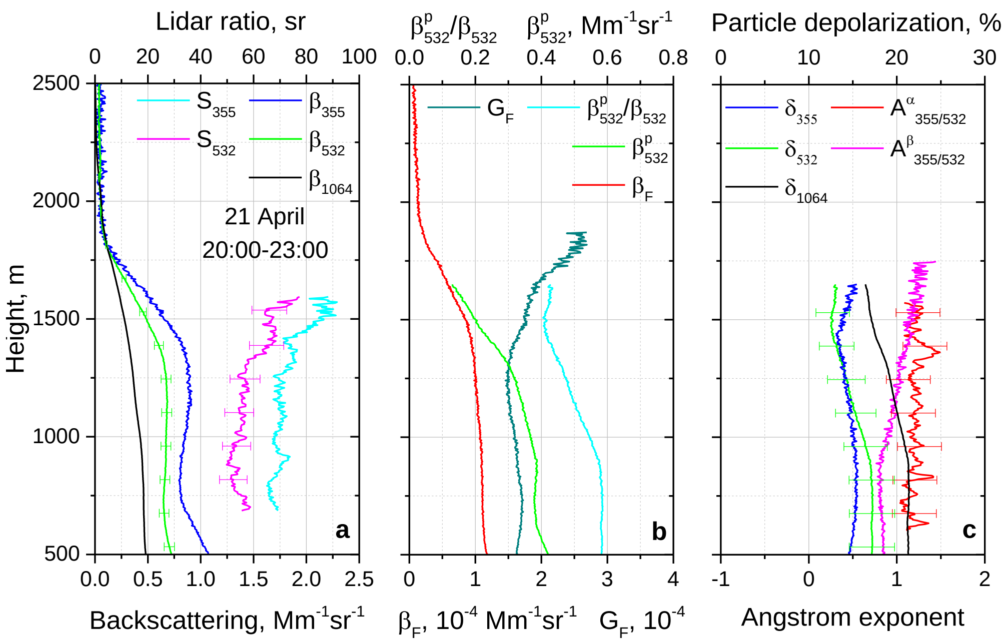

Fig.11. The same particle parameters as in Fig.10 for 21 April 2020, 20:00-23:00 UTC. Measurements were performed at 30 deg to horizon.

https://doi.org/10.5194/amt-2021-80
Preprint. Discussion started: 24 March 2021

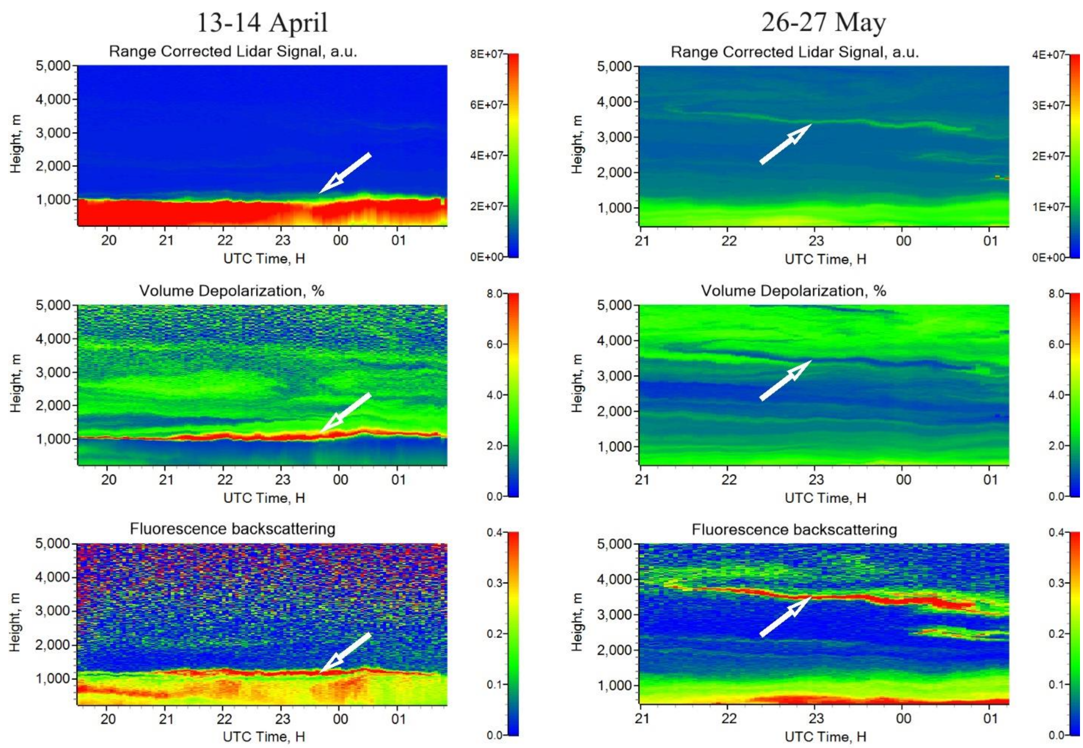

Fig.12. Range corrected lidar signal at 1064 nm, volume depolarization ratio δ^{v}_{1064} and fluorescence backscattering coefficient (in 10^{-4} $Mm^{-1}sr^{-1}$) measured on 13-14 April (left column) and 26-27 May 2020 (right column). Arrows point to the fluorescent layers.

https://doi.org/10.5194/amt-2021-80
Preprint. Discussion started: 24 March 2021

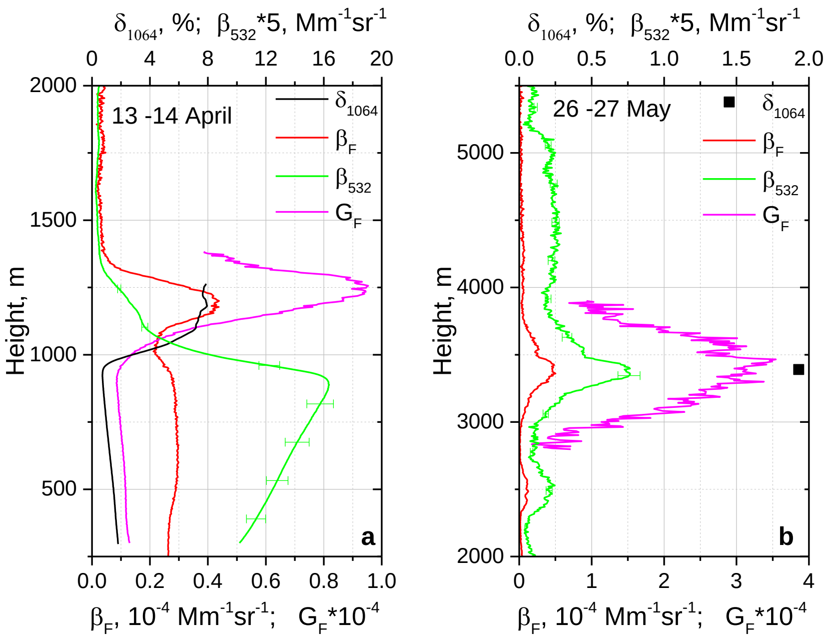

Fig.13. Vertical profiles of elastic β_{532} and fluorescence β_F backscattering coefficients, fluorescence capacity G_F and particle depolarization ratio δ_{1064} measured on (a) 13-14 April for 21:00 – 01:00 UTC and (b) 26-27 May 2020 for 23:30 – 00:40 UTC. Values of β_{532} are multiplied by factor 5.

https://doi.org/10.5194/amt-2021-80
Preprint. Discussion started: 24 March 2021

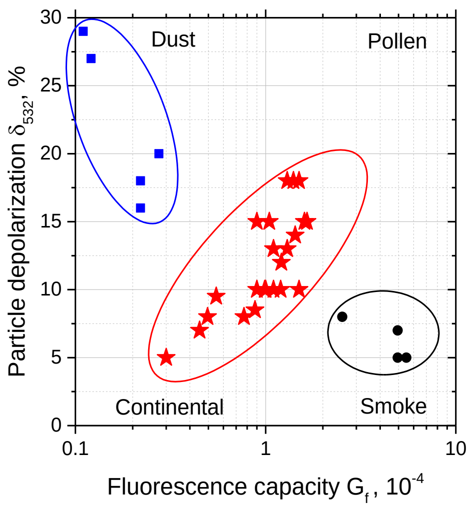

Fig.14. Particle depolarization δ_{532} versus fluorescence capacity G_F. This diagram allows to identify dust (blue), smoke particles (black) and aerosol mixtures containing pollen (red).